F. Colombi, A. Colagrossi, M. Lavagna
Characterisation of 6DOF Natural and Controlled Relative Dynamics in Cislunar Space
Acta Astronautica, In press - Published online 15/01/2021
doi:10.1016/j.actaastro.2021.01.017

Characterisation of 6DOF Natural and Controlled Relative Dynamics in Cislunar Space

Francesco Colombi[a,*], Andrea Colagrossi[b], Michèle Lavagna[c]

[a] *M.Sc. Graduate in Space Engineering, Politecnico di Milano, Via La Masa 34, 20156 Milano - Italy*
[b] *Postdoctoral Research fellow, Department of Aerospace Science and Technology, Politecnico di Milano, Via La Masa 34, 20156 Milano - Italy*
[c] *Full Professor, Department of Aerospace Science and Technology, Politecnico di Milano, Via La Masa 34, 20156 Milano - Italy*

Abstract

At the 50th anniversary of Apollo 11, the Moon is back to the scene of scientific and commercial space exploration interests. During the next decade, the establishment of a Gateway in cislunar non-Keplerian orbits will open the space frontiers to sustainable manned and robotic missions on and around the Moon. Such infrastructure will require several logistic operations for its assembly and maintenance, which lean on rendezvous and docking capabilities. Even if few missions have flown on non-Keplerian orbits, Rendezvous and Docking (RV&D) operations have not been performed but in Low Earth Orbit (LEO). Investigations about 6 Degrees Of Freedom (DOF) relative dynamics in non-Keplerian environment are now mandatory to highlight criticalities in the design of the cislunar gateway and to translate RV&D protocols, consolidated in LEO for the International Space Station (ISS), to the new non-Keplerian environment. In this direction, the paper analyses the 6DOF natural orbit-attitude dynamics within the Circular Restricted Three-Body Problem (CR3BP) framework. A novel perspective of the dynamical structures, constituting 6DOF manifolds, allows to better characterise the natural relative dynamics in proximity of non-Keplerian orbits. The importance of orbit-attitude manifolds exploitation is underlined for designing reliable and efficient rendezvous trajectories, enhanced by natural cislunar dynamics.

Then, an ephemeris cislunar dynamical model is exploited to address guidance laws for proximity operations. The control capability is included in the dynamics of a chaser vehicle, which is employed to solve the 6DOF guidance problem in proximity of a target spacecraft. The results obtained with the controlled dynamics are compared to those available thanks to natural motion, discussing the energetic and time costs to complete the manoeuvres. A control parametrization to solve the optimal energy rendezvous problem is proposed.

Finally, a feasible operational rendezvous scenario is discussed about the identified favourable locations along the non-Keplerian orbit to perform complex proximity operations. Significant relations between RV&D time and non-Keplerian orbit's period are discussed as well.

Keywords: Orbit-attitude Relative Dynamics, Orbit-attitude Manifolds, Optimal Energy Control, Cislunar Space, Near Rectilinear Halo Orbit (NRHO).

1. Introduction

Space agencies belonging to the International Space Exploration Coordination Group (ISECG), partners in collaboration at the International Space Station (ISS), have endorsed plans to establish a new permanent space asset orbiting in Moon vicinity. A cislunar gateway, also known as Lunar Orbital Platform-Gateway (LOPG) or Deep Space Gateway (DSG), represents a fundamental step in the sustainable, reusable, long-term architecture to support the next generation of human and robotic

*Corresponding author
Email addresses: colombi.francesco93@gmail.com (Francesco Colombi), andrea.colagrossi@polimi.it (Andrea Colagrossi), michelle.lavagna@polimi.it (Michèle Lavagna)

space exploration and commercial mission on and around the Moon. It is offering a relatively accessible testbed to develop technologies and operations in preparation for deep space exploration which will ultimately brings human to Mars [1, 2]. Such space infrastructure shall ensure significant flexibility in order to support different robotics and manned missions. A fundamental functionality of the Gateway will be the possibility of frequent docking/undocking events of different space vehicle classes, such as the Orion spacecraft or the lunar service module. Moreover, many logistic operations will be required for the establishment and maintenance of this permanent modular infrastructure, leveraging on autonomous Rendezvous and Docking (RV&D) proximity operations of multiple station modules.

Recent studies have selected Earth-Moon Near Rectilinear Halo Orbit (NRHO) as the most attractive staging orbit candidate for the lunar gateway [3]. Thus, this orbital family will be the focus of this investigation.

Rendezvous operations between two spacecraft in Low Earth Orbit (LEO) have been extensively studied and tested in the past years, especially thanks to the ISS programme. Back to the years of Apollo programme, relative motion and rendezvous manoeuvres in Low Lunar Orbit (LLO) have been accomplished. However, no proximity manoeuvring has been actually performed so far in a multi-body gravitational environment, such as the cislunar space.

Despite non-Keplerian multi-body dynamics is well known and it has been exploited in several trajectory design and optimisation studies for low-energy transfer and station-keeping applications (e.g. in the Earth-Moon system [4, 5]), the integration of the relative dynamics of such multi-body gravitational environment in the design of Guidance, Navigation and Control (GNC) systems is recent and sometimes overlooked. Several studies about relative dynamics and proximity motion in the Circular Restricted Three-Body Problem (CR3BP) was applied to formation flying by Marchand, Héritier and Howell [6, 7]. Within the same dynamical model, simple rendezvous strategies based on targeting methods were proposed by Lizy-Destrez and Murakami [8, 9]. More recently, different researches have started to analyse and propose rendezvous strategies focusing on cislunar multi-body environment, as in the work of Mammarella [10] and Blazquez [11]. However, literature is often missing a careful dynamical modelling of cislunar environment, or a complete 6 Degrees Of Freedom (DOF) orbit-attitude analysis.

The earliest studies concerning the attitude stability of a satellite within the CR3BP were conducted by Kane et al. [12] and Robinson [13], assuming a satellite artificially maintained at the location of the libration points. More recently, Brucker et al. [14] explored the attitude dynamics and stability of a spacecraft fixed at the equilibrium point location in the Sun-Earth system by exploiting Poincaré maps; Wong et al. [15] extended the analysis of attitude motion for a single rigid body orbiting on linearised Lyapunov and Halo orbits in the Sun-Earth system. The general coupling between orbital and attitude dynamics in CR3BP was introduced by Guzzetti [16] and Colagrossi [17], who provided families of orbit-attitude periodic solutions. The formalization of orbit-attitude relative dynamics in multi-body gravitational cislunar environment was just recently proposed by Colagrossi and Lavagna [18].

This paper aims to present an overall characterisation of the coupled 6DOF natural and controlled relative dynamics of two rigid bodies orbiting in a multi-body gravitational regimes such as the cislunar space, with particular focus on Near Rectilinear Halo Orbits. The eigen-structures of the manifolds, known in the classical CR3BP, have been extended to their coupled orbit-attitude representation, highlighting and discussing the dynamical features of orbital and attitude modes. Those coupled structures, previously introduced by the authors [19], have been investigated under a new relative perspective to deeply describe the orbit-attitude natural dynamics characterising the relative translational and rotational motion in proximity of reference periodic solutions in the 6DOF space. The useful insight outcomes from the natural analysis have been used as a base in the characterisation analyses of the continuous controlled relative cislunar dynamics, which aims to define simple guidance and control functions for both orbital and rotational components.

The novel results about relative dynamics characterization with orbit-attitude natural manifolds are applied to evaluate 6DOF controlled proximity manoeuvres, which minimise the control effort leveraging the peculiarities of the multi-body gravitational dynamics in lunar vicinity. In these regards, the paper proposes new guidance and control laws based on simple polynomial functions and ap-

plies them to solve the minimal energy rendezvous problem. The results obtained imposing various initial and final condition have been summarised, and their general behaviours are presented. The available results on controlled relative trajectories are critically discussed with respect to the natural manifolds characterisation introduced by the research work presented in this paper.

Finally, a feasible rendezvous scenario to the cislunar Gateway is proposed synthesising the outcomes of both natural and controlled characterisation analyses.

2. Dynamical Models and Assumptions

The paper discusses natural and controlled 6DOF relative motions of two rigid bodies in cislunar space, under the combined gravitational action of the Earth and the Moon. The dynamical modelling to describe both orbital and attitude relative states is fundamental to analyse proximity operations, as well as accurate formation flying, in this peculiar gravitational environment.

The paper considers both natural and controlled 6DOF relative dynamics. The former is analysed within a CR3BP model, while the latter makes use of a more refined Ephemeris 3-body model. This is motivated by the fact that results and conclusions about natural dynamics characterisation, under CR3BP assumptions, can be easily extended to a more refined dynamical model, which supports the investigation on controlled dynamics, since it is more closely related to practical applications requiring high accuracy models.

2.1. Relative Orbit-Attitude CR3BP Model

The analysis of the natural relative 6DOF motion is carried out within the simplified framework of the CR3BP. It represents the simplest orbital model able to catch the main features of the attractive non-Keplerian multi-body cislunar environment. The Euler's rotation equations are included into the classical CR3BP dynamics, so that the orbit-attitude motion can be propagated simultaneously [17].

The CR3BP describes the motion of a spacecraft m, under the gravitational attraction of m_1 and m_2. The spacecraft is assumed as a rigid body, with negligible mass with respect to the primaries ($m \ll m_1, m_2$). Within CR3BP simplification, the primaries move on circular orbits about their common barycentre with constant angular velocity Ω_s.

The study of the relative dynamics involves two independent spacecraft, which are labelled as target, with mass m_T, and chaser, with mass m_C.

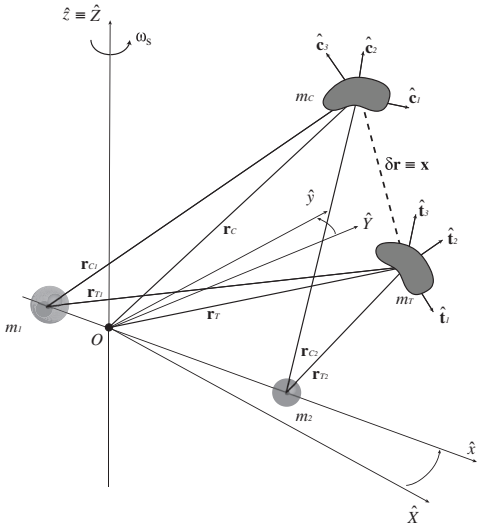

Figure 1: Orbit-attitude absolute and relative model.

A rotating synodic $\{\hat{r}\}$-frame is conveniently defined to analyse the absolute and relative CR3BP motion of the spacecraft. As can be seen in figure 1, this non-inertial frame is centred at the barycentre of the Earth-Moon system, O, and it is aligned with the reference inertial $\{\hat{i}\}$-frame at the time $t = 0$. Its $\hat{\boldsymbol{x}}$-axis is directed from m_1 to m_2 and its $\hat{\boldsymbol{z}}$-axis is in the direction of the angular velocity of the primaries, $\boldsymbol{\omega_s} = \Omega_s \hat{\boldsymbol{z}}$, while the $\hat{\boldsymbol{y}}$-axis completes the triad. The equation of motion can be conveniently normalised via the definition of characteristic quantities, so that the distance between the two primaries r_{12}, the synodic angular velocity Ω_s and the total mass of the system $m_1 + m_2$ are unitary in non-dimensional units (symbol [ndim]). By doing so, the system becomes uniquely described by the mass parameter μ.

$$\mu = \frac{m_2}{m_1 + m_2} \tag{1}$$

The absolute orbital states $\boldsymbol{x_{orb}} = \{\boldsymbol{r}; \boldsymbol{v}\} = [x; y; z; v_x; v_y; v_z]$ describe the position and the velocity of the centre of mass of the two spacecraft, $\boldsymbol{x_{orb_T}}$ and $\boldsymbol{x_{orb_C}}$, which are expressed in the $\{\hat{r}\}$-frame. The attitude quaternions $\boldsymbol{q_T}$ and $\boldsymbol{q_C}$ parametrise the orientation of the body-fixed frames with respect to the $\{\hat{i}\}$-frame. The body-fixed frames of the spacecraft, $\{\hat{b}_T\} = \{\hat{\boldsymbol{t}}_1, \hat{\boldsymbol{t}}_2, \hat{\boldsymbol{t}}_3\}$

and $\{\hat{b}_C\} = \{\hat{\boldsymbol{c}}_\mathbf{1}, \hat{\boldsymbol{c}}_\mathbf{2}, \hat{\boldsymbol{c}}_\mathbf{3}\}$, are located at the centre of mass of the corresponding spacecraft and they are aligned with their principal inertia directions. The angular rates, $\boldsymbol{\omega_T}$ and $\boldsymbol{\omega_C}$, relative to the $\{\hat{i}\}$-frame and expressed in the respective body-fixed frames, complete the attitude states of the spacecraft.

In previous works of the authors [19, 20], the perturbation effect of the attitude motion on the orbital dynamics resulted negligible for present or near-future spacecraft operating in cislunar space. The order of magnitude of the net perturbation force, which is exerted on a spacecraft due to its finite extended dimension, with respect to its point-mass simplification is proportional to the following relation.

$$\|\boldsymbol{f}_{pert_i}\| \sim \left(\frac{l^\star_{SC}}{r_i}\right)^2, \tag{2}$$

In this formulation the length of the spacecraft is labelled as $l^\star_{SC}$ and it is intrinsically linked to the ratio between the spacecraft inertial moments and mass; the distance from the i-th primary body is r_i. For example, considering a spacecraft with characteristic length equal to 100 meters, the perturbation magnitude will range from $\mathcal{O}(10^{-9})$ (at perilune of an NRHO) to $\mathcal{O}(10^{-12})$ (at apolune of an NRHO). This perturbation is many order of magnitude lower with respect to other perturbation sources in the Earth-Moon system, such as the gravitational presence of the Sun [21]. Thus, the orbital dynamics has been modelled via the classical CR3BP equations. Conversely, the rotational dynamics is coupled to the orbital one, being driven by the gravity gradient torques of the two primaries on the spacecraft [17, 16].

By defining r_1 and r_2 as the distance of the generic spacecraft (e.g. valid for both target and chaser) from the first and second primary, respectively, the classical CR3BP dynamical equations can be defined as follows.

$$\boldsymbol{f}_{\text{CR3BP}} = \begin{cases} \dot{x} = & v_x \\ \dot{y} = & v_y \\ \dot{x} = & v_x \\ \dot{v}_x = & x + 2v_y - \dfrac{(1-\mu)(x+\mu)}{{r_1}^3} \\ & -\dfrac{\mu(x-1+\mu)}{{r_2}^3} \\ \dot{v}_y = & y - 2v_x - \dfrac{(1-\mu)y}{{r_1}^3} - \dfrac{\mu y}{{r_2}^3} \\ \dot{v}_z = & -\dfrac{(1-\mu)z}{{r_1}^3} - \dfrac{\mu z}{{r_2}^3} \end{cases} \tag{3}$$

The Euler equations of rotational dynamics are defined as follows.

$$\boldsymbol{f}_\omega = \begin{cases} \dot{\omega}_1 = \dfrac{I_3 - I_2}{I_1} & \dfrac{3(1-\mu)}{{r_1}^5} g_2 g_3 \\ & \left. + \dfrac{3\mu}{{r_2}^5} h_2 h_3 - \omega_2\omega_3 \right) \\ \dot{\omega}_2 = \dfrac{I_1 - I_3}{I_2} & \dfrac{3(1-\mu)}{{r_1}^5} g_1 g_3 \\ & \left. + \dfrac{3\mu}{{r_2}^5} h_1 h_3 - \omega_1\omega_3 \right) \\ \dot{\omega}_3 = \dfrac{I_2 - I_1}{I_3} & \dfrac{3(1-\mu)}{{r_1}^5} g_1 g_2 \\ & \left. + \dfrac{3\mu}{{r_2}^5} h_1 h_2 - \omega_1\omega_2 \right) \end{cases} \tag{4}$$

The inertia matrix of the generic spacecraft is $\mathbb{I} = diag[I_1, I_2, I_3]$, being the body-fixed $\{\hat{b}\}$-frame aligned to its principal inertia axes. It should be noticed that the orbital dynamics enters in the terms g_i and h_i, which represents the direction cosines of the radial vector going from the i-th primary to the spacecraft, expressed in the body-fixed $\{\hat{b}\}$-frame.

The quaternion kinematic equations are added to complete the orbit-attitude dynamics.

$$\boldsymbol{f}_q = \begin{cases} \dot{q}_1 = & \frac{1}{2}\left(\omega_3 q_2 - \omega_2 q_3 + \omega_1 q_4\right) \\ \dot{q}_2 = & \frac{1}{2}\left(-\omega_3 q_1 + \omega_1 q_3 + \omega_2 q_4\right) \\ \dot{q}_3 = & \frac{1}{2}\left(\omega_2 q_1 - \omega_1 q_2 + \omega_3 q_4\right) \\ \dot{q}_4 = & \frac{1}{2}\left(-\omega_1 q_1 - \omega_2 q_2 - \omega_3 q_3\right) \end{cases} \tag{5}$$

The integration of these equations returns the evolution of the attitude quaternion ${}^{\hat{i}}\boldsymbol{q}^{\hat{b}} = [q_1; q_2; q_3; q_4]$ and angular velocity ${}^{\hat{i}}\boldsymbol{\omega}^{\hat{b}} = [\omega_1; \omega_2; \omega_3]$. Note that,

during numerical integration, the quaternion constraint has to be always satisfied:

$$q_1{}^2 + q_2{}^2 + q_3{}^2 + q_4{}^2 = 1. \tag{6}$$

The resulting set of differential equations constituting the system can be resumed as follows.

$$\begin{cases} \dot{\boldsymbol{x}}_{\boldsymbol{orb}} & = \boldsymbol{f}_{\mathrm{CR3BP}}(\boldsymbol{x}_{\boldsymbol{orb}}) \\ {}^{\hat{i}}\dot{\boldsymbol{q}}^{\hat{b}} & = \boldsymbol{f}_q({}^{\hat{i}}\boldsymbol{q}^{\hat{b}},\, {}^{\hat{i}}\boldsymbol{\omega}^{\hat{b}}) \\ {}^{\hat{i}}\dot{\boldsymbol{\omega}}^{\hat{b}} & = \boldsymbol{f}_\omega(\boldsymbol{x}_{\boldsymbol{orb}},\, {}^{\hat{i}}\boldsymbol{q}^{\hat{b}},\, {}^{\hat{i}}\boldsymbol{\omega}^{\hat{b}}). \end{cases} \tag{7}$$

Once the absolute 6DOF states of both target and chaser spacecraft are available from the numerical propagation of the dynamics in eq. (7), the relative orbit-attitude states between the chaser and the target spacecraft can be directly obtained thanks to the relative kinematic relations [18]. Relative position, $\boldsymbol{x} \equiv \delta\boldsymbol{r}$, is defined as follows.

$$\delta\boldsymbol{r}(t) = \boldsymbol{r_C}(t) - \boldsymbol{r_T}(t) \tag{8}$$

The relative attitude quaternion $\delta\boldsymbol{q}$ can be obtained by applying the rule of successive rotation for quaternions:

$$\delta\boldsymbol{q}(t) = {}^{\hat{b}_T}\boldsymbol{q}^{\hat{b}_C}(t) = \boldsymbol{q_T}{}^{-1}(t) \odot \boldsymbol{q_C}(t) \tag{9}$$

In this notation $\odot$ is the quaternion left product operator. The rotation matrix $[\delta C] = [C_{\hat{b}_T/\hat{b}_C}]$, which transform a vector from the target body-fixed $\{\hat{b}_T\}$-frame to the chaser body-fixed $\{\hat{b}_C\}$-frame, directly follows from $\delta\boldsymbol{q}$. Finally, the relative angular velocity $\delta\boldsymbol{\omega}^{\hat{b}_C}$ between the two spacecraft can be defined as it is seen in the chaser body-fixed $\{\hat{b}_C\}$-frame.

$$\delta\boldsymbol{\omega}^{\hat{b}_C}(t) = \boldsymbol{\omega_C}(t) - [\delta C]\,\boldsymbol{\omega_T}(t). \tag{10}$$

As a result, the relative rotational dynamics referring to $\{\hat{b}_T\}$ non-inertial reference frame, expressed in the chaser body-fixed $\{\hat{b}_C\}$-frame, can be formulated in the vectorial form by the following equation:

$$\begin{aligned} \delta\dot{\boldsymbol{\omega}}^{\hat{b}_C} = \mathbb{I}_C^{-1}\Bigg\{ & -\Big[\delta\boldsymbol{\omega}^{\hat{b}_C}\times\Big]\,\mathbb{I}_C\,\delta\omega^{\hat{b}_C} \\ & -\Big[\delta\boldsymbol{\omega}^{\hat{b}_C}\times\Big]\,\mathbb{I}_C[\delta C]\,\boldsymbol{\omega_T} + \mathbb{I}_C\,\Big[\delta\boldsymbol{\omega}^{\hat{b}_C}\times\Big]\,[\delta C]\,\boldsymbol{\omega_T} \\ & -\Big[[\delta C]\boldsymbol{\omega_T}\times\Big]\mathbb{I}_C\,\delta\boldsymbol{\omega}^{\hat{b}_C} + \boldsymbol{N_C} - [\delta C]\Big[\\ & \Big([\delta C]^T\mathbb{I}_C[\delta C] - \mathbb{I}_T\Big)\mathbb{I}_T^{-1}\Big(\boldsymbol{N_T} - [\boldsymbol{\omega_T}\times]\,\mathbb{I}_T\,\boldsymbol{\omega_T}\Big) \\ & + [\boldsymbol{\omega_T}\times]\,\Big([\delta C]^T\mathbb{I}_C[\delta C] - \mathbb{I}_T\Big)\boldsymbol{\omega_T}\Big] - [\delta C]\boldsymbol{N_T}\Bigg\} \end{aligned} \tag{11}$$

This compact formulation is obtained by the definition of the skew-symmetric cross-product matrix operator $[\boldsymbol{u}\times]$. The torques $\boldsymbol{N_C}$ and $\boldsymbol{N_T}$ are the total torques acting on chaser and target spacecraft, expressed in their corresponding reference body-fixed frame [22, 23]. In CR3BP, these torques are composed by the gravity gradients due to the two primaries.

2.2. Relative Orbit-Attitude Ephemeris Model

Although CR3BP represents a valuable and powerful tool in preliminary analysis, higher-fidelity models are fundamental to support later stages of space mission design, especially for RV&D and proximity operations GNC applications.

In this paper, an ephemeris dynamical model has been employed to analyse the controlled dynamics during proximity operations of target and chaser spacecraft operating along non-Keplerian cislunar orbits, such as NRHO. The gravitational presence of the Sun, as well as the actual orbits of the Earth and the Moon are the most relevant perturbation in cislunar environment, which have been neglected in the previous CR3BP simplification. The employment of numerical ephemeris data gathered via the SPICE Toolkit offered by NASA/JPL allows to include the actual motion of the Earth, the Moon and the Sun in the ephemeris dynamical model. Also the Solar Radiation Pressure (SRP) has been included in the orbit-attitude ephemeris dynamics, whose effect is modelled considering the spacecraft as a composition of multiple flat surfaces. The total SRP perturbation force and torque are obtained by summing up each contribution of the illuminated surfaces of the spacecraft.

In this case, the orbit-attitude dynamical framework is an ephemeris four-body problem. Differently from the CR3BP formulation, the orbit-attitude ephemeris model is conveniently expressed in the inertial reference $\{\hat{i}\}$-frame. For example, the absolute orbital dynamics of the target spacecraft in ephemeris model is described in vectorial form as follows.

$$\begin{aligned} \ddot{\boldsymbol{r}}^{\hat{\boldsymbol{i}}}{}_T = & -\frac{\mu_1}{{r_{T1}}^3}\boldsymbol{r}^{\hat{\boldsymbol{i}}}_{\boldsymbol{T1}} - \frac{\mu_2}{{r_{T2}}^3}\boldsymbol{r}^{\hat{\boldsymbol{i}}}_{\boldsymbol{T2}} + \\ & -\mu_S\left(\frac{\boldsymbol{r}^{\hat{\boldsymbol{i}}}_{\boldsymbol{T\,S}}}{{r_{T\,S}}^3} + \frac{\boldsymbol{r}^{\hat{\boldsymbol{i}}}_{\boldsymbol{S2}}}{{r_{S2}}^3}\right) + \boldsymbol{a}^{\hat{\boldsymbol{i}}}_{\boldsymbol{SRP}}. \end{aligned} \tag{12}$$

The gravitational planetary parameters of Earth, Moon and Sun are respectively written as μ_1, μ_2

and μ_S; the vector $\boldsymbol{r}_{\boldsymbol{T}}^{\hat{\boldsymbol{i}}}$ is the position of the target spacecraft in the inertial $\{\hat{i}\}$-frame; $\boldsymbol{a}_{\boldsymbol{SRP}}^{\hat{\boldsymbol{i}}}$ is the SRP acceleration term.

The relative orbital states can be obtained by differentiating the absolute states, as in eq. (8), or by directly integrating the relative orbital dynamics. In this case, being referred with respect to the inertial $\{\hat{i}\}$-frame, it is directly obtained from the differences between the translational accelerations acting on the chaser, $\ddot{\boldsymbol{r}}_{\boldsymbol{C}}^{\hat{\boldsymbol{i}}}$, and the target spacecraft, $\ddot{\boldsymbol{r}}_{\boldsymbol{T}}^{\hat{\boldsymbol{i}}}$, .

$$\ddot{\boldsymbol{x}}^{\hat{\boldsymbol{i}}} = \delta\ddot{\boldsymbol{r}}^{\hat{\boldsymbol{i}}} = \ddot{\boldsymbol{r}}_{\boldsymbol{C}}^{\hat{\boldsymbol{i}}} - \ddot{\boldsymbol{r}}_{\boldsymbol{T}}^{\hat{\boldsymbol{i}}} \tag{13}$$

The absolute and relative rotational dynamics in the ephemeris model have the same form of equations (4) and (11), but now they are rewritten considering the actual position of the primaries, and including also the perturbation terms of Sun gravity, as fourth body, and of SRP. In particular, the torques $\boldsymbol{N_C}$ and $\boldsymbol{N_T}$ are now constituted by the gravity gradient torques due to the Moon, Earth and Sun, and by the SRP torque acting on each spacecraft.

Further details about the development of the orbit-attitude ephemeris four-body problem dynamics can be found in previous works of the authors [17, 18, 20].

3. Orbit-Attitude Natural Relative Dynamics

The invariant manifolds represent a primary tool to investigate the natural dynamics characterising the Libration Point Orbit (LPO)s and, in particular, the relative motion in their immediate proximity. This chapter analyses the manifolds associated to NRHOs, in their orbit-attitude extension, employing the simplified CR3BP dynamical model described in section 2.1. These informations gives helpful insights for the design of natural and/or low-energy proximity operations in the cislunar environment considering the 6DOF motion of the spacecraft.

3.1. Orbit-Attitude Relative Modes

Periodic rotational behaviours respect the synodic $\{\hat{r}\}$-frame, associated to a well-known periodic LPO existing in the CR3BP, can be discovered from the study of the orbit-attitude dynamics (7). Peculiar natural dynamical structures exist around these equilibrium periodic solutions, which may be classified in stable, unstable, periodic and center invariant manifolds [24]. In the classical CR3BP, the manifolds have been widely explored in their absolute point of view, such as consistent low-energy transfer possibilities to and among many LPOs [25].

Starting from the variational equation obtained via Taylor expansion of the dynamics (7), the fundamental matricial differential equation of the State Transition Matrix (STM) is obtained.

$$\dot{\Phi}(t,t_0) = A(t)\Phi(t,t_0) \quad \text{with} \quad \Phi(t_0,t_0) = I_{12\times 12} \tag{14}$$

In the initial boundary condition, the STM is equal to the 12-by-12 identity matrix, $I_{12\times 12}$. The STM $\Phi(t,t_0)$ constitutes the linear mapping of the variation of the orbit-attitude state at time t due to an initial variation of the reference state at time t_0. Further details about the dynamical model, such as the definition of each term composing the Jacobian $A(t)$, or numerical methods to find periodic solutions, can be found in [16]. According to the Floquet's theory, the stability information and the local direction of the invariant manifolds constituting the eigenstructure surrounding the neighbourhood of a reference periodic solution are embedded into the STM after a full LPO period T, which matrix is also known as monodromy matrix. It should be highlighted that the monodromy matrix $M = \tilde{\Phi}(T,0)$ has to fully reflect the point of view of a rotating observer sitting in the synodic $\{\hat{r}\}$-frame for both the orbital and attitude states. From the eigenanalysis of the monodromy matrix, 6 orbital modes and 6 attitude modes can be distinguished. The eigenvalues λ_j of the monodromy matrix are related to the departure rate of the mode, while the eigenvectors $\boldsymbol{e_j}$ describe the relative "local" direction of the corresponding invariant manifolds in the 12-dimensional space of the orbit-attitude dynamics.

The numerical method employed in this paper explores the 12-dimensional surfaces of the orbit-attitude invariant manifolds via discretisation. The periodic orbit-attitude LPO is discretised in N points. The n-th point along the LPO is identified by the corresponding time $t_n = T(n-1)/N$. The Floquet modes $\boldsymbol{e_j}$ are propagated to the n-th point through the STM seen from a fixed observer respect the synodic $\{\hat{r}\}$-frame.

$$\boldsymbol{v_j} = \tilde{\Phi}(t_n, 0)\, \boldsymbol{e_j} \tag{15}$$

Each propagated mode $\boldsymbol{v_j}$ represents the ap-

proximated "local" direction of the corresponding "global" invariant manifold (i.e. periodic, stable, unstable or center) expressed in the synodic point of view for both orbital and attitude motion. A small perturbation along the direction of the eigenmode $\boldsymbol{v_j}$ moves the spacecraft onto the 12-dimensional surface of the "global" orbit-attitude invariant manifold from the nominal periodic orbit solution. The desired equivalent magnitude of perturbation can be non-dimensionalised considering the corresponding characteristic dimension of the CR3BP system. For example, an equivalent perturbation magnitude in the position component can be non-dimensionalised by the characteristic length of the Earth-Moon system. It is important to remark that a good numerical approximation of the manifold will be obtained by employing lower values of the perturbation magnitude ε. To correctly find the initial point to propagate the orbit-attitude manifolds, the perturbation has to be added coherently to the full orbit-attitude states $\boldsymbol{X}(t_n)$ of the LPO.

$$\begin{cases} \boldsymbol{x_{orb_m}}(t_n) & = \boldsymbol{x_{orb}}(t_n) + \varepsilon\, \delta \boldsymbol{v_j}_{1:6} \\ {}^{\hat{i}}\boldsymbol{q_{1:3_m}}^{\hat{b}}(t_n) & = {}^{\hat{i}}\boldsymbol{q_{1:3}}^{\hat{b}}(t_n) + \varepsilon\, \delta \boldsymbol{v_j}_{7:9} \\ {}^{\hat{i}}\boldsymbol{\omega_m}^{\hat{b}}(t_n) & = {}^{\hat{i}}\,\boldsymbol{\omega}^{\hat{b}}(t_n) + \varepsilon\, \delta \boldsymbol{v_j}_{10:12}, \end{cases} \tag{16}$$

where ${}^{\hat{i}}\boldsymbol{q_{1:3}}^{\hat{b}} = [q_1; q_2; q_3]$ are the vector components of the quaternion vector.

Note that the attitude states are expressed with respect the inertial $\{\hat{i}\}$-frame in the dynamics equations (7), and particular attention must be paid to the quaternion perturbation direction. First, the attitude quaternion ${}^{\hat{i}}\boldsymbol{q}^{\hat{b}}$ is transformed to the body quaternion with respect to the synodic $\{\hat{r}\}$-frame, ${}^{\hat{r}}\boldsymbol{q}^{\hat{b}}$. In this way, the attitude quaternion is expressed according to Floquet modes periodic formulation. Then, the manifold perturbation can be added to ${}^{\hat{r}}\boldsymbol{q}^{\hat{b}}$, hence q_4 is derived from the quaternion constraint relation in eq. (6). Finally, the quaternion is converted back to the inertial $\{\hat{i}\}$-frame to obtain a perturbed state that can be directly propagated through the developed orbit-attitude dynamics.

This section presents a case study on a cislunar L1 Northern NRHO with vertical amplitude $A_z \simeq 78.1 \times 10^3$ km ($\simeq 0.2031$ [ndim]) and orbital period $T \simeq 8.15$ days ($\simeq 1.8760$ [ndim]). A librating periodic behaviour about the synodic $\{\hat{r}\}$-frame for the rotational motion of the cislunar Gateway has been chosen (e.g. no complete rotation in an orbital period), as relevant particular case of periodic attitude natural solution within the 6DOF dynamics.

3.2. Approaching/Departing Natural Trajectories

The stable and unstable manifolds constitute reliable and robust natural reference corridors for a chaser spacecraft (such as cargo or crewed vehicles, station modules, lunar service vehicle, etc.), which can be respectively exploited in approaching operations to a target (e.g. the cislunar Gateway) or departing procedures (e.g. from the Gateway after undocking).

Figure 2 shows the relative trajectories belonging to the stable orbital manifold seen in the synodic $\{\hat{r}\}$-frame point of view. The 6DOF natural dynamics has been propagated over 2-orbital periods (about 16 days), considering as insertion points of the chaser spacecraft (drawn with circled dots) different initial locations along the reference LPO, which are equispaced in phase angle. The black line depicts the path followed by the stable mode starting from a manifold insertion at the apolune of the NRHO. Typically, the stable manifold trajectories are obtained via reverse-time propagation. However, they are propagated forward to explore the actual relative motion of the approaching modes.

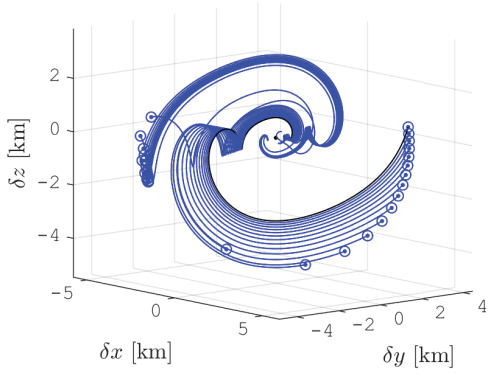

Figure 2: Relative orbital dynamics over 2-orbital periods of stable orbital mode trajectories. Earth-Moon L_1 northern NRHO with $A_z \simeq 78.1 \times 10^3$ km ($\simeq 0.2031$ [ndim]). Initial chaser offset of 5 km.

The chaser is assumed to begin its approach from 5 km distance. After the first full period it has reduced the distance to about 1 km, and after the second period it reaches a distance close to 300 m. In proximity of the reference solution, all the orbital modes maintains the same structure even if the initial offset distance at the insertion point is different. For example, starting from 50 km for the same

reference NRHO, after the first period the distance becomes about 11 km and after the second period it is in the order of 3 km. It should be highlighted that the distance between target and chaser has a steep variation at each perilune passage, whose magnitude is related to the stability of the LPO. This exponential step-like evolution is quite characteristic of all NRHOs, having a dynamically sensible perilune region and a quieter apolune region. An example of this sensitivity can be appreciated in figure 2, looking at the relative trajectory obtained by the insertion point just after the perilune passage (i.e. the trajectory not grouped with other similar relative trajectories). In fact, the "local" direction of the manifold is more difficult to accurately approximate near the perilune region

The unstable trajectories describe a similar dynamical structure of the stable one, but they are travelling in the opposite direction and it eventually diverges departing from the target. Figure 3 reports the relative trajectories belonging to the unstable orbital manifold of the reference NRHO seen in the synodic $\{\hat{r}\}$-frame point of view. The chaser departs from 200 m initial offset distance along the unstable mode and the natural drift is propagated over 2-orbital periods.

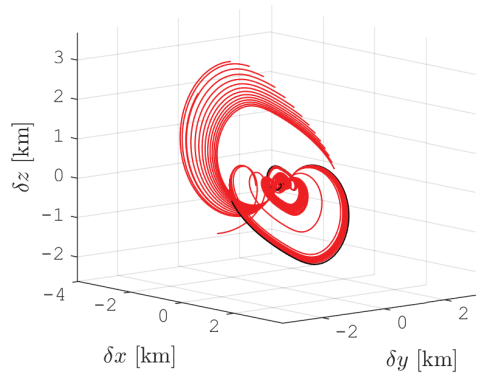

Figure 3: Relative orbital dynamics over 2-orbital periods of unstable orbital mode trajectories. Earth-Moon L_1 northern NRHO with $A_z \simeq 78.1 \times 10^3$ km ($\simeq 0.2031$ [ndim]). Initial chaser offset of 200 m.

The typical surface structure of the stable and unstable manifolds belonging to NRHOs is constituted by two opposite conical-spiralling regions which are connected to each other by wide arches. Exiting from one of the slow apolune conical-spiralling region, the relative orbital dynamics of the trajectories quickly evolves on the wide curve reaching its maximum velocity in correspondence of the perilune. Then, the relative dynamics on the wide curve progressively slows down while target and chaser approach the apolune. It eventually enters a new slowly spiralling motion on the opposite cone of the manifold. Then, a new cycle begins.

3.3. Bounded Natural Trajectories

The center orbital invariant manifolds contain the remaining characteristics dynamics of the non-Keplerian multi-body orbits and they describe bounded relative motions in proximity of the reference periodic orbit-attitude LPO. For any periodic orbit-attitude solution in the CR3BP, a couple of unitary eigenvalues exists for both orbital and rotational behaviour. The corresponding eigenmodes are labelled as periodic modes because their motion is associated to the periodicity behaviours of the reference LPO. Finally, if a couple of eigenvalues of the monodromy matrix M lays on the unitary circle in the complex plane, a couple of "center" eigenmodes will span the surface in the 12-dimensional orbit-attitude space. This eigenstructure identifies quasi-periodic behaviour in proximity of the periodic reference solution.

The relative trajectories with a drop-like shape shown in figure 4 correspond to the relative motions of a chaser lying on the periodic orbital mode, labelled as P1, for five different insertion location along the reference NRHO with an initial offset of 200 m. This relative motion represents a temporal shift along the same periodic orbit-attitude LPO between the chaser and target spacecraft. For this reason, the relative motion is closer to the target in the apolune region, while the distance reaches its maximum at perilune passage where the dynamics is faster and the same temporal displacement corresponds to a greater distance.

The nature of this mode offers a useful relative periodic orbit that can be leveraged as safe checkpoints during the approaching phases of RV&D operations. For example, a chaser spacecraft could lay on it, waiting for the authorisation to proceed its proximity operations.

The last class of orbital modes is represented by the center orbital modes, which dynamics develops in complex hovering relative motions of the chaser spacecraft around the target. The particular case shown in figure 5 corresponds to the propagation over 6-orbital period after a manifold insertion happening at apolune of a center orbital mode. This motion is associated to the first orbital mode of the

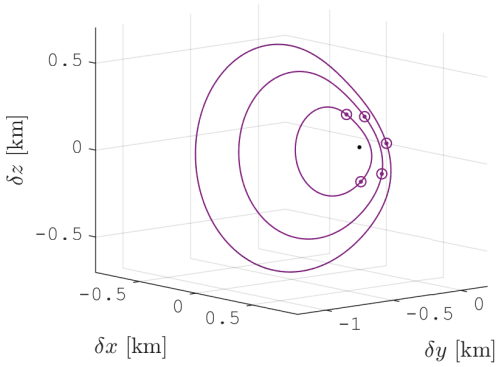

Figure 4: Relative orbital dynamics over 2-orbital periods of periodic orbital mode trajectories. Earth-Moon L_1 northern NRHO with $A_z \simeq 78.1 \times 10^3$ km ($\simeq 0.2031$ [ndim]). Initial chaser offset of 200 m.

the couple of center eigenmodes and it has been labelled as C1. The chaser maintains a safe distance from the target spacecraft, ranging from 100 m to 1.8 km after an insertion along the center mode at 200 m.

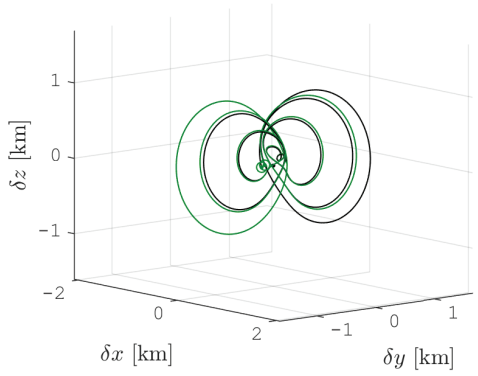

Figure 5: Relative orbital dynamics over 6-orbital periods of center orbital mode trajectories. Earth-Moon L_1 northern NRHO with $A_z \simeq 78.1 \times 10^3$ km ($\simeq 0.2031$ [ndim]). Initial chaser offset of 200 m.

The wide arcs composing the center mode behaviour are characteristic of NRHOs, direct consequence of the close passage to the Moon. An oscillating behaviour having a longer period respect the orbit characterises these particular orbital dynamical structures, which resembles the oscillating behaviour observed in literature for NRHO [26].

The black line corresponds to the mode obtained by the insertion at apolune at time $t = 0$, while the green line represents an apolune insertion happening along the same eigenmode after one orbital period. Both the insertion has been computed to be at initial distance equivalent to 200 m. The small displacement between the two line is due to the quasi-periodic dynamical evolution of the center mode, which continuously modifies the equivalent magnitude of the projection along the instantaneous "local" direction of the mode.

3.4. Natural Attitude Motions on Orbital Modes

Discussing about the shape of the orbit-attitude modes in the 12-dimensional space, it should be highlighted how the 6 orbital modes include a significant component in both the orbital and attitude subspaces due to the cross-coupling determined by the gravity gradient torque. On the contrary, the remaining 6 attitude modes are constituted by the solely attitude component. The existence of these purely attitude modes is directly linked to the adopted simplification of the dynamical model, where attitude variations do not affect the spacecraft trajectory.

Figure 6 shows the relative attitude motion of the chaser moving along two different natural orbital modes: the stable and periodic orbital modes shown before, respectively in figure 2 and figure 4). The relative attitude is analysed in comparison with the relative distance evolution.

As can be observed in figure 6, the natural attitude of the chaser moving along the orbital modes remains synchronised (e.g. null relative attitude states) to the one of the target spacecraft on the reference solution. This synchronisation is kept when the chaser remain below a certain relative distance, which is in the order of hundreds of kilometres ($\sim 10^{-4}[ndim]$) considering the case of NRHO. This behaviour has been observed for all the orbital modes of LPOs in the Earth-Moon system, but the actual limiting distance to keep the synchronization changes depending on the nature of the orbit.

The synchronised relative attitude motion on natural orbit-attitude trajectories is a relevant result, which can be beneficially exploited while analysing and designing controlled relative 6DOF motion in non-Keplerian multi-body orbits. In fact, along a natural relative trajectory, the attitude of the chaser remains aligned with the one of the target.

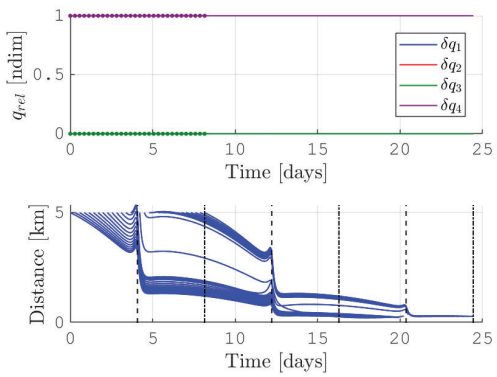

(a) Stable orbital mode

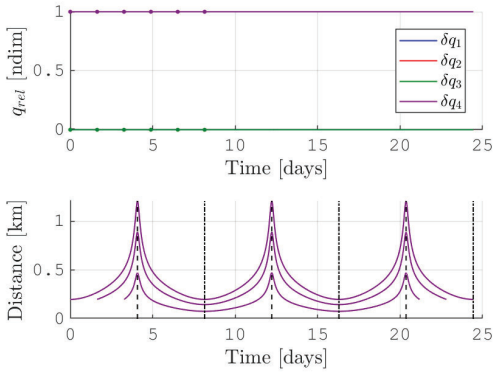

(b) Periodic orbital mode

Figure 6: Relative attitude dynamics of orbital modes over 2-orbital periods, in relation with the relative distance. Earth-Moon L_1 northern NRHO with $A_z \simeq 78.1\times10^3$ km ($\simeq 0.2031$ [ndim]).

4. Orbit-Attitude Controlled Relative Dynamics

Orbit-attitude controlled relative dynamics in cislunar space is relevant to any space application that requires complex RV&D or proximity operations. In fact, despite the influence of natural motion is significant in multi-body gravitational environment, the presence of unmodelled perturbations, uncertainties or GNC errors make necessary the presence of active control systems. Nevertheless, the characterisation of natural relative dynamics, discussed in section 3, can be conveniently exploited within the guidance functions for trajectory design. In fact, approaching, departing or hovering trajectories are naturally possible thanks to stable, unstable, periodic and center manifolds, respectively. The dynamical informations obtained in the CR3BP analysis can be coherently extended in the ephemeris models as initial guess.

As already said, the controlled dynamics has been investigated leveraging the ephemeris four-body problem described in section 2.2. This is motivated by the accuracy typically required in practical GNC applications.

According to the analysis about the natural relative motion of the chaser, the dynamically quiet apolune region of NRHOs has been identified as the most favourable environment to perform complex controlled proximity operations, such as the approaching phases to finalise the docking to the lunar Gateway [27]. Therefore, the apolune has been assumed as a representative initial point for the relative control discussion presented in this section.

Although any space mission is a complex system engineering problem, dealing with several requirements and constraints from any subsystem, the guidance and control problem is here defined within the optimal energy context, to asses the feasibility of control proximity operations in cislunar space with minimum control energy. This choice allows to better highlight the exploitation of natural relative manifolds highlighted in section 3.

4.1. Direct Transcription of Relative Guidance

In the assumed scenario, the target spacecraft (e.g. the lunar Gateway) is a passive vehicle maintaining its nominal non-Keplerian cislunar orbit, while the chaser spacecraft is an active vehicle with complete orbit-attitude control capability. The analysis does not consider the actuation problem; therefore, the output control function is the nominal vector of linear accelerations $\boldsymbol{a_C}$ expressed in the inertial $\{\hat{i}\}$-frame and the nominal vector of angular acceleration $\boldsymbol{\alpha_C}$ expressed in the chaser body-fixed $\{\hat{b}_C\}$-frame. The control action $\boldsymbol{u}(t) = [\boldsymbol{a_C}; \boldsymbol{\alpha_C}]$ is included in the relative dynamical model, equation (13) and the ephemeris version of equation (11), as additional external force and torque terms acting on the chaser spacecraft or, equivalently, as translational and rotational acceleration additional terms.

$$\begin{cases} \ddot{\tilde{\boldsymbol{x}}}^{\hat{i}} & = \ddot{\boldsymbol{x}}^{\hat{i}} + \boldsymbol{a_C} \\ \delta\dot{\tilde{\boldsymbol{\omega}}}^{\,\hat{b}_C} & = \delta\dot{\boldsymbol{\omega}}^{\,\hat{b}_C} + \boldsymbol{\alpha_C} \end{cases} \tag{17}$$

The proximity guidance Optimal Control Problem (OCP) is reduced to a Non-Linear Programming (NLP) problem by parametrizing the control variable and by transcribing the dynamical system

(17) and its boundaries into a finite set of equality constraints. In this analysis, the 6DOF controlled trajectory has been not discretised in multiple arcs connected by patch points. Therefore, the control parametrisation will have to offer a greater flexibility than a simple linear function, while maintaining a reduced complexity to limit the dimension of the NLP. Moreover, the optimisation has been decided to be performed over different fixed Time Of Flight (TOF), t_f. As a consequence, only the parameters which characterise the control actions of the chaser constitute the vector of unknown variables $\boldsymbol{p}$, solution of the NLP.

The final relative orbit-attitude state $\boldsymbol{X}(t_f)$ at the end of the controlled rendezvous simulation has to satisfy a set of desired boundary conditions. Null relative position and velocities, as well as attitude states correspond to the simplest docking condition which can be analysed.

$$\begin{cases} \boldsymbol{x}(t_f) & = [0;0;0] \\ \dot{\boldsymbol{x}}(t_f) & = [0;0;0] \\ \boldsymbol{q}(t_f) & = [0;0;0;\pm 1] \\ \boldsymbol{\omega}(t_f) & = [0;0;0] \end{cases} \tag{18}$$

In practical rendezvous scenarios, the position vector of the docking hatch will be likely displaced from the center of mass of the target spacecraft. It follows the docking boundary condition at time $t = t_f$ will be related to the 6DOF configuration of the space gateway driven by its absolute orbit-attitude dynamics. In general, the final desired 6DOF states of the chaser spacecraft will be a function of the 6DOF states of the target states and t_f. The definition of an error state vector $[\delta\boldsymbol{x};\delta\boldsymbol{v};\delta\boldsymbol{q};\delta\boldsymbol{\omega}]$ between the relative orbit-attitude state of the chaser and a desired final relative condition $[\boldsymbol{x_d};\boldsymbol{v_d};\boldsymbol{q_d};\boldsymbol{\omega_d}]$ allows to generalise the boundary conditions (18) to any controlled relative 6DOF motion problem.

$$\begin{cases} \delta\boldsymbol{x} & = \boldsymbol{x}(t_f) - \boldsymbol{x_d} \\ \delta\boldsymbol{v} & = \dot{\boldsymbol{x}}(t_f) - \boldsymbol{v_d} \\ \delta\boldsymbol{q} & = \boldsymbol{q_d}^{-1} \odot \boldsymbol{q}(t_f) \\ \delta\boldsymbol{\omega} & = \boldsymbol{\omega}(t_f) - \boldsymbol{\omega_d} \end{cases} \tag{19}$$

The actual configuration of the chaser and target spacecraft can be directly included in the final boundary condition. This would be obtained by means of coordinate transformations, e.g. to derive the relative 6DOF states between the active docking mechanism of the chaser and the passive docking ring of the target Gateway.

Different parametrisation possibilities are viable for the controlled dynamics. Favourable results have been obtained by the authors employing polynomial and Fourier series [18]. The latter is used for rotational dynamics control to guarantee numerical convergence to the optimal solution. A simpler version of control parametrisation is proposed in this paper, where a second degree polynomial parametrisation is shown to be robust enough for the translational control $\boldsymbol{a_C}$. Also with this novel parametrisation, the rotational dynamics requires more parameters to achieve numerical convergence: a third degrees polynomial function has been used to parametrise $\boldsymbol{\alpha_C}$.

$$\boldsymbol{a_C}(\boldsymbol{p},t) = \boldsymbol{a_0} + \boldsymbol{a_1}\left(\frac{t}{t_{ref}}\right) + \boldsymbol{a_2}\left(\frac{t}{t_{ref}}\right)^2 \tag{20}$$

$$\boldsymbol{\alpha_C}(\boldsymbol{p},t) = \boldsymbol{\alpha_0} + \boldsymbol{\alpha_1}\left(\frac{t}{t_{ref}}\right) + \boldsymbol{\alpha_2}\left(\frac{t}{t_{ref}}\right)^2 + \boldsymbol{\alpha_3}\left(\frac{t}{t_{ref}}\right)^3 \tag{21}$$

The parameters $\boldsymbol{a_i}$ and $\boldsymbol{\alpha_i}$ are 3×1 vectors which constitute the control variable $\boldsymbol{p} = \{\boldsymbol{a_i};\boldsymbol{\alpha_i}\}$. Their physical dimensions are determined by the physical quantity they are parametrizing. The reference time t_{ref} is required to non-dimensionalise the time during the manoeuvre t. The final form of the control action $\boldsymbol{u}(\boldsymbol{p},t)$ is obtained by including the control functions (20) and (21).

$$\boldsymbol{u}(\boldsymbol{p},t) = \begin{Bmatrix} \boldsymbol{a_C}(\boldsymbol{p},t) \\ \boldsymbol{\alpha_C}(\boldsymbol{p},t) \end{Bmatrix} \tag{22}$$

In this case, the dimension of the problem is 21, where 9 parameters are used for translational control and 12 parameters define the rotational one. Note that the control action profile, as well as the evolution of the controlled orbit-attitude dynamics, is defined for the full manoeuvre once the parameters $\boldsymbol{a_i}$ and $\boldsymbol{\alpha_i}$ of $\boldsymbol{p}$ are fixed.

The objective of the guidance algorithm is to find a control profile $\boldsymbol{u}(\boldsymbol{p},t)$ to perform the continuously controlled proximity manoeuvre through a constrained optimisation of a performance index J. In general, any performance function can be formulated by a terminal penalty term φ and a Lagrangian term $\mathcal{L}$.

$$J = \varphi(\boldsymbol{x}_f, t_f) + \int_{t_0}^{t_f} \mathcal{L}\left(\boldsymbol{x}(t), \boldsymbol{u}(t), t\right) dt \tag{23}$$

The terminal penalty term will be not considered in this investigation, because the NLP has been formulated to consider the final boundary condition as a constraint in the optimisation. Therefore, the performance index in equation (23) is defined according to the Lagrangian formulation for the optimal energy proximity guidance (i.e. minimum quadratic control) as a function of the control variable $\boldsymbol{p}$.

$$J(\boldsymbol{p}) = \frac{1}{2}\int_{t_0}^{t_f} \boldsymbol{u}^T(\boldsymbol{p},t)\,\boldsymbol{u}(\boldsymbol{p},t)\,dt \qquad (24)$$

The NLP is solved through a constrained minimisation algorithm which exploits the Sequential Quadratic Programming (SQP) method.

4.2. General Continuous Guidance Results

The study aims to provide a general characterisation of controlled relative dynamics in cislunar space. Hence, random initial relative orbit-attitude states, as well as representative departure locations along the stable or unstable modes, or along other locations conveniently identified by the natural dynamics characterisation (e.g. periodic manifold), have been explored for the chaser spacecraft. Different final offset position with final attitude synchronisation have been investigated, obtaining similar results.

For example, figure 7 shows the guidance functions obtained for a representative far-range rendezvous problem (i.e. initial relative distance in the order of 10^2 km).

The example rendezvous TOF is quite shorter with respect to the characteristic period of the natural dynamics of the NRHO (and more in general of non-Keplerian cislunar orbits), where target and chaser spacecraft are orbiting. For example, the terminal RV&D sequence should be completed within few hours or at maximum two days (i.e. in line with the operational requirements established during the ISS experience). Instead, the orbital period of the NRHO lasts about 7-8 days. Therefore, the deviations from the natural dynamics have not enough time to affect significantly the optimal energy guidance control.

The optimal energy guidance progressively evolves from the departure acceleration to the final deceleration, exploiting at the most the inertial natural motion in the middle of the manoeuvre. The guidance control force is almost linear, although it has been parametrised through a second order polynomial function, as expected from the quadratic formulation of the optimal energy problem.

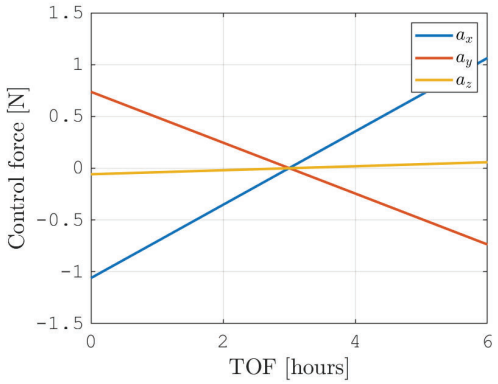

(a) Control force. Chaser mass $m_C \sim 10^3$ kg

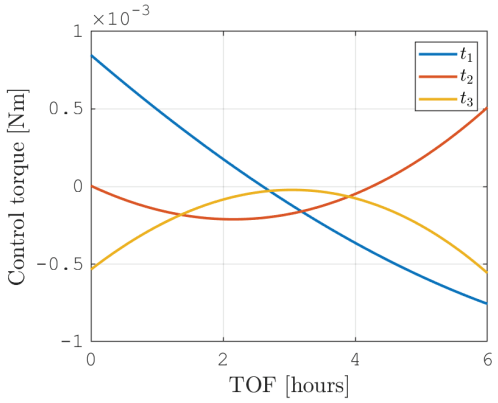

(b) Control torque. Chaser inertia $\mathbb{I}_C \sim 10^4$ kgm^2

Figure 7: Direct transcription control of the 6DOF rendezvous guidance NLP. Rendezvous TOF $t_f = 6$ hours. Spacecraft inertia properties: $m_C \sim 10^3$ kg; $\mathbb{I}_C \sim 10^4$ kgm^2. Case with random initial relative states for far-range RV&D.

This result is independent from the initial offset position direction and from the attitude dynamics. The translational guidance cost only depends on the initial distance of the chaser from the target desired destination, the initial relative velocity of the chaser, and from the TOF requested to perform the manoeuvre.

The control torques tend to use the higher order terms of the control parametrisation. Even if it should be highlighted that the optimal energy guidance tends to use slow relative angular velocity profiles to synchronise the initial attitude offset for longer rendezvous TOF, by exploiting the natural attitude dynamics existing in cislunar space. When the initial relative angular velocity is smaller enough with respect to the natural synchronised rate, the control torque behaviour will be almost

linear. Vice versa, if the initial relative angular velocity of the chaser is comparable, such as in figure 7, or higher to the optimal natural synchronisation rate, the control torque function will present relevant higher-order terms.

An important outcome concerns the small magnitude of the control action requested by the 6DOF guidance of a quite large chaser spacecraft ($\sim 10^3$ kg). It suggests the equipment of a 6DOF control system independent from the main engines, requiring a sensible throttling capability. This could be made through a dedicated cluster of manoeuvring thrusters or angular momentum control devices, such as reaction wheels.

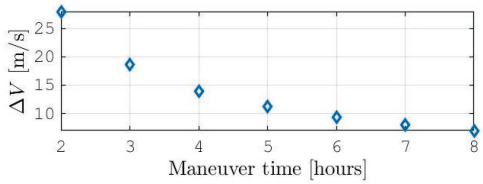

(a) Translational control effort

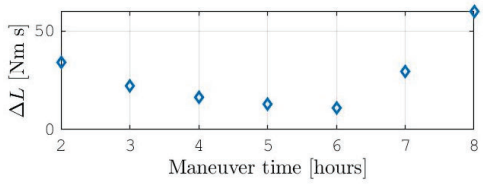

(b) Rotational control effort

Figure 8: Rendezvous control effort in relation to the manoeuvre TOF, t_f. Spacecraft inertia properties: $m_C \sim 10^3$ kg; $\mathbb{I}_C \sim 10^4$ kgm^2. Initial relative states as in figure 7.

The same manoeuvre scenarios shown in figure 7 has been solved for different reasonable TOF to compare the control effort requirements. Figure 8 reports the control effort to perform a far-range rendezvous starting at a distance of 70 km, with an injection velocity error of few cm/second and executing a large-slew manoeuvre. The point solution with TOF equal to 6 hours corresponds to the case shown in figure 7.

In general, the optimal energy translational guidance results in lower control costs for longer rendezvous TOF. In fact, the guidance and control functions are able to spread their control actions more effectively, having a longer time to complete the manoeuvre within the natural dynamics regime. This is not true for the rotational dynamics control, which struggles on convergence when the rendezvous TOF are too long. This is related to a more complex evolution of the control torque to avoid departure from the natural synchronised motion. For these limiting cases, the optimal energy rotational guidance is more prone to reach the final relative attitude configuration through overshooting or additional rotations, which result in non-linear control functions and higher control costs (see figure 8(b)).

This conclusion can be further analysed looking at figure 9, where the evolution of the relative quaternion of the chaser with respect to the target and the control torque are reported. The initial condition for this solution are the same of the previously presented case in figure 7, but now the time to complete the manoeuvre has been increased to 7 hours. A more complex attitude control torque is evident, with larger attitude oscillations along the rendezvous trajectory.

5. Rendezvous and Docking Strategy

Given the natural and controlled relative dynamics characterisation results discussed in the previous section, an example rendezvous and docking strategy implementation is here discussed.

For what concern the implementation of the proposed methods, the absolute and relative ephemeris orbit-attitude dynamics, in chapter 2, can be numerically propagated with on-board computers exploiting pre-saved look-up tables of the ephemerides. In this way, the computational load is suitable for on-board applications [28]. The chaser and/or the target spacecraft will have available relative and absolute navigation measurements. For example, the chaser is expected to be equipped with relative navigation sensors (e.g. LIght Detection And Ranging (LIDAR), vision-based technologies) for 6DOF state determination [29, 30]. The target spacecraft is expected to be passive, but cooperative, during the rendezvous operations, and it shall have an additional relative state determination system for safety reasons [31]. Moreover, both spacecraft shall have an absolute navigation system based on a ground-tracking measurements, such as the Deep Space Network (DSN) [32].

The chaser vehicle is assumed to reach the proximity operation distance from the target space infrastructure during a phasing phase prior the rendezvous. The chaser has to arrive approximately at 100 km distance from the target well before the NRHO apolune [27]. In this way, the navigation

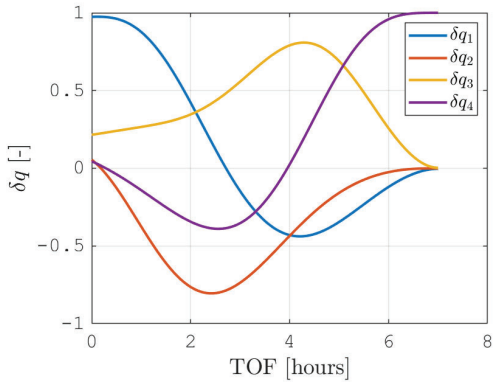

(a) Controlled relative quaternion evolution. Chaser inertia $\mathbb{I}_C \sim 10^4$ kgm^2

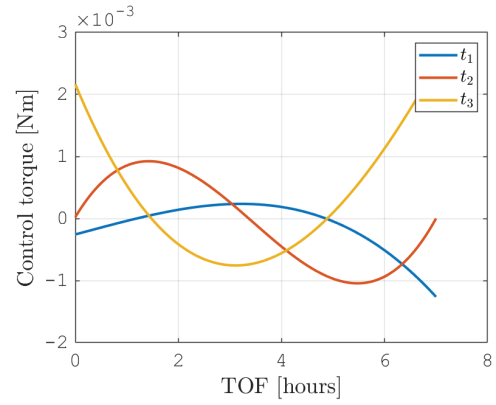

(b) Control torque. Chaser inertia $\mathbb{I}_C \sim 10^4$ kgm^2

Figure 9: Direct transcription control of the 6DOF rendezvous guidance NLP. Rendezvous TOF $t_f = 7$ hours. Spacecraft inertia properties: $m_C \sim 10^3$ kg; $\mathbb{I}_C \sim 10^4$ kgm^2. Initial relative states as in figure 7.

system has enough time to perform accurate orbital determination and data processing [33].

A communication/telemetry link between the chaser spacecraft and the target Gateway can be established. Communication capabilities between the two vehicles may be required for operational and safety reasons, as well as for navigation functionalities. The proximity communication infrastructure is assumed to be analogous to the one already implemented for ISS proximity operations, e.g. via S-band antenna [34]. The end of the phasing phase is assumed to happen when the hand-over from absolute to relative navigation is successfully achieved.

At this point, the chaser vehicle begins the far-range rendezvous phase with its insertion onto the stable orbital manifold of the NRHO. This insertion point has been calculated before, during the orbital determination procedure. This choice allows to exploit a natural approaching trajectory to reduce the active control effort. The proposed guidance laws enable a control strategy over the natural manifolds to manage this rendezvous phase. In fact, the chaser vehicle will perform small Maintenance Correction Maneuvers (MCM) in order to follow the natural dynamics of the approaching path described by the stable orbital mode. After a full orbital period (about 8 days) on this mode, the chaser vehicle acquires a relative distance in the order of 10 km from the target space infrastructure.

The short-range phase constitutes the final part of the RV&D procedure. During this phase, the chaser vehicle is guided through several predetermined checkpoints by the GNC system. The optimal energy rendezvous guidance algorithm can be employed to compute the continuous relative 6DOF function for the orbit-attitude guidance. Then, a closed-loop control system will drive the on-board actuation devices of the chaser (e.g. thrusters and reaction wheels) to maintain nominal condition during the approach. A simple operational scenario is proposed to include two checkpoints, as already discussed by the authors in [27]. Exiting from the stable orbital manifold, the chaser will move towards the first Waiting Point (WP1), which is place on the unstable orbital manifold at 1 km distance from the target space infrastructure. The second checkpoint (WP2) has been placed 200 meters away the target, again on the unstable orbital manifold. In this way, the chaser spacecraft will naturally drift away from the target avoiding the possibility of a collision. This will ensure passive safety if any anomaly occurs, e.g. engine failure. Periodic and center manifold directions can be exploited in case hovering is sought in the rendezvous operations.

During the closing approach stage, the chaser moves from WP1 to WP2 while it will perform an attitude rotation manoeuvre which has to establish the alignment of the docking mechanisms in preparation of the final translation along the R-bar towards the docking ring of the gateway. This manoeuvre can follow an optimal energy control path. During the Final Translation Stage, the attitude of the chaser has to be maintained synchronized with the one of the target to not break the correct pointing between the docking mechanism and the target's docking port. This can be easily achieved by exploiting the coupled attitude dynamics over the natural orbital manifolds, as in section 3.4.

6. Conclusions

This paper focuses its analysis on the problem of a space vehicle performing proximity operations, characterising natural relative motions existing in the cislunar gravitational environment and assessing the guidance and control capabilities of the spacecraft with simple polynomial functions. The outcomes of the investigation have been applied to a strategy to carry out the final Rendezvous and Docking (RV&D) operations to a cislunar target, possibly operating on a Near Rectilinear Halo Orbit (NRHO) around the Moon. The RV&D strategy proposed in this study is based on the design of checkpoints the chaser spacecraft has to pass through during the final approaching phase, exploiting at maximum the natural characteristics of the multi-body gravitational environment.

During this analysis the quiet and wide apolune region of NRHO has been identified as favourable location to perform these complex controlled proximity manoeuvres. Useful approaching/departing natural corridors to and from the target space station, as well as bounded natural hovering trajectories around the target has been highlighted thanks to the Floquet's modes. Moreover, the synchronised attitude motion on natural orbit-attitude trajectories has been discussed, with focus on possible favourable extensions to controlled dynamics applications. It should be underlined that all these natural motions are featured by a constrained path, which is defined by the natural manifolds, and by a characteristic time equal to the orbital period of the NRHO (i.e. about 8 days). The analysis of the orbit-attitude manifold under the relative dynamics perspective allowed a direct application to proximity operations design.

In practical scenarios, the natural dynamics only may result too constraining to design entire sets of proximity operations. The long time associated to natural motion may suggest to beneficially exploit the controlled dynamics. An optimal energy relative guidance, based on simple polynomial functions has been presented, discussing 6DOF controlled dynamics of the chaser along proximity trajectories. The controlled motion can be applied to move from a checkpoint to the next one, following trajectories which are characterised by a middle section with almost natural drift dynamics, and synchronising the relative attitude to keep the correct pointing configuration.

It should be noticed that the configuration of the lunar Gateway is still to be defined. Future developments of that project could lead to new more complex operational constraints, such as path limitations for RV&D or proximity operations. However, the flexibility of the proposed methodology, based on natural relative dynamics and optimal energy relative guidance, allows to overcome this kind of limitations in the future developments of the proposed methods.

7. Acknowledgements

The work was performed under the cap of activities related to the Agenzia Spaziale Italiana - Politecnico di Milano Agreement "Ricerca e Innovazione" N.2018-H.0.

References

[1] ISECG, The global exploration roadmap, Tech. rep., International Space Exploration Coordination Group (2018).

[2] R. W. Farquhar, D. W. Dunham, Y. Guo, J. V. McAdams, Utilization of libration points for human exploration in the sun–earth–moon system and beyond, Acta Astronautica 55 (3-9) (2004) 687–700. doi:10.1016/j.actaastro.2004.05.021.

[3] R. Whitley, R. Martinez, Options for staging orbits in cislunar space, in: 2016 IEEE Aerospace Conference, IEEE, Big Sky, MT, USA, 2016, pp. 1–9. doi:10.1109/AERO.2016.7500635.

[4] D. C. Folta, M. Woodard, K. Howell, C. Patterson, W. Schlei, Applications of multi-body dynamical environments: The ARTEMIS transfer trajectory design, Acta Astronautica 73 (2012) 237–249. doi:10.1016/j.actaastro.2011.11.007.

[5] D. C. Folta, N. Bosanac, D. Guzzetti, K. C. Howell, An Earth-Moon system trajectory design reference catalog, Acta Astronautica 110 (2015) 341–353. doi:10.1016/j.actaastro.2014.07.037.

[6] B. G. Marchand, K. C. Howell, Control strategies for formation flight in the vicinity of the libration points, Journal of Guidance, Control, and Dynamics 28 (6) (2005) 1210–1219. doi:10.2514/1.11016.

[7] A. Héritier, K. C. Howell, Dynamical evolution of natural formations in libration point orbits in a multi-body regime, Acta Astronautica 102 (2014) 332–340. doi:10.1016/j.actaastro.2013.10.017.

[8] S. Lizy-Destrez, Rendezvous optimization with an inhabited space station at EML2, in: 25th International Symposium on Space Flight Dynamics (ISSFD), Munich, Germany, 2015.

[9] N. Murakami, S. Ueda, T. Ikenaga, M. Maeda, T. Yamamoto, H. Ikeda, Practical rendezvous scenario for transportation missions to cis-lunar station in earth-moon l2 halo orbit, in: 25th International Symposium on Space Flight Dynamics (ISSFD), Munich, Germany, 2015.

[10] M. Mammarella, E. Capello, G. Guglieri, Robust Model Predictive Control for Automated Rendezvous Maneuvers in Near-Earth and Moon Proximity, 2018. doi:10.2514/6.2018-5343.

[11] E. Blazquez, L. Beauregard, S. Lizy-Destrez, Safe natural far Rendezvous approaches for Cislunar Near Rectilinear Halo orbits in the Ephemeris model, 2018.

[12] T. R. Kane, E. L. Marsh, Attitude stability of a symmetric satellite at the equilibrium points in the restricted three-body problem, Celestial mechanics 4 (1) (1971) 78–90. doi:10.1007/BF01230323.

[13] W. J. Robinson, Attitude stability of a rigid body placed at an equilibrium point in the restricted problem of three bodies, Celestial mechanics 10 (1) (1974) 17–33. doi:10.1007/BF01261876.

[14] E. Brucker, P. Gurfil, Analysis of gravity-gradient-perturbed rotational dynamics at the collinear lagrange points, The Journal of the Astronautical Sciences 55 (3) (2007) 271–291. doi:10.1007/BF03256525.

[15] B. Wong, R. Patil, A. Misra, Attitude Dynamics of Rigid Bodies in the Vicinity of the Lagrangian Points, Journal of Guidance, Control, and Dynamics 31 (1) (2008) 252–256. doi:10.2514/1.28844.

[16] D. Guzzetti, K. C. Howell, Natural periodic orbit-attitude behaviors for rigid bodies in the three-body periodic orbits, ACTA Astronautica 130 (2016) 97–113. doi:10.1016/j.actaastro.2016.06.025.

[17] A. Colagrossi, M. Lavagna, Preliminary results on the dynamics of large and flexible space structures in halo orbits, ACTA Astronautica 134 (2017) 355–367. doi:10.1016/j.actaastro.2017.02.020.

[18] A. Colagrossi, M. Lavagna, Cislunar non-keplerian orbits rendezvous and docking: 6dof guidance and control, 69th International Astronautical Congress, 1-5 October 2018, Bremen, Germany (2018).

[19] A. Colagrossi, M. Lavagna, Assembly and operations for a cisluna orbit space station, in: 68th International Astronautical Congress, 25-29 September 2017, Adelaide, Australia, 2017.

[20] F. Colombi, Characterization of relative 6DOF natural and controlled dynamics in cislunar space, Master's thesis, Politecnico di Milano (Apr. 2019).
URL https://www.politesi.polimi.it/retrieve/383306/2019_04_Colombi.pdf

[21] L. Bucci, Coupled orbital-attitude dynamics of large structures in non-keplerian orbits, Master's thesis, Politecnico di Milano (2015).

[22] G. Q. Xing, S. A. Parvez, Relative attitude kinematics and dynamics equations and its applications to spacecraft attitude state capture and tracking in large angle slewing maneuvers, Tech. rep., MIT Lincoln Laboratory, Lexington, Massachusetts (1999).

[23] G. Q. Xing, S. A. Parvez, Alternate forms of relative attitude kinematics and dynamics equations, in: 2001 Flight Mechanics Symposium, 2001.

[24] L. Perko, Differential Equations and Dynamical Systems, Springer, 2001.

[25] W. S. Koon, M. W. Lo, J. E. Marsden, S. D. Ross, Dynamical Systems: the Three-Body Problem and Space Mission Design, Marsden Books, 2008. doi:10.1142/9789812792617_0222.

[26] D. Guzzetti, E. M. Zimovany, K. C. Howell, D. C. Davis, Stationkeeping analysis for spacecraft in lunar near rectilinear halo orbits, in: 27th AAS/AIAA Space Flight Mechanics Meeting, 5-9 February 2017, San Antonio, Texas, USA, 2017.

[27] L. Bucci, A. Colagrossi, M. Lavagna, Rendezvous in lunar near rectilinear halo orbits, Advances in Astronautics Science and Technology 1 (1) (2018) 39–43. doi:10.1007/s42423-018-0012-6.

[28] P. Seidelmann, L. Doggett, P. Janiczek, Algorithms, calculators, and computers for celestial navigation, Proceedings of the IEEE 71 (10) (1983) 1201–1204. doi:10.1109/proc.1983.12749.

[29] C. D. Souza, T. Crain, F. Clark, J. Getchius, Orion cislunar guidance and navigation, in: AIAA Guidance, Navigation and Control Conference and Exhibit, American Institute of Aeronautics and Astronautics, 2007. doi:10.2514/6.2007-6681.

[30] H. Hinkel, S. Cryan, C. D'Souza, M. Strube, NASA's Automated Rendezvous and Docking Sensor Development and its Applicability to the GER, in: Space Exploration International Conference, Strasbourg, France, 2014.
URL https://ntrs.nasa.gov/archive/nasa/casi.ntrs.nasa.gov/20140013499.pdf

[31] C. D. Souza, C. Hannak, P. Spehar, F. Clark, M. Jackson, Orion rendezvous, proximity operations and docking design and analysis, in: AIAA Guidance, Navigation and Control Conference and Exhibit, American Institute of Aeronautics and Astronautics, 2007. doi:10.2514/6.2007-6683.

[32] D. Curkendall, J. Border, Delta-DOR: The One-Nanoradian Navigation Measurement System of the Deep Space Network — History, Architecture, and Componentry, in: Interplanetary Network Progress Report, Vol. 42-193, 2013, pp. 1–46.
URL https://ui.adsabs.harvard.edu/abs/2013IPNPR.193D...1C

[33] S. Muñoz, J. Christian, E. G. Lightsey, Development of an end to end simulation tool for autonomous cislunar navigation, in: AIAA Guidance, Navigation, and Control Conference, American Institute of Aeronautics and Astronautics, 2009. doi:10.2514/6.2009-5995.

[34] R. Dempsey, ISS: Operating an Outpost in the New Frontier, National Aeronautics and Space Administration, 2018.
URL http://www.nasa.gov/connect/ebooks/the-international-space-station-operating-an-outpost